International Forum on Aeroelasticity and Structural Dynamics
IFASD 2024
17-21 June 2024, The Hague, The Netherlands

AEROELASTIC HYBRID TESTING FOR INDUSTRIAL APPLICATIONS

Davide Balatti[1], Hamed Haddad Khodaparast[1], Shakir Jiffri[1], Michael I. Friswell[1], Sebastiano Fichera[2], Alessandra Vizzaccaro[3], Andrea Castrichini[4]

[1]Swansea University
Fabian Way, Crymlyn Burrows, Skewen, Swansea SA1 8EN
davide.balatti@swansea.ac.uk

[2]University of Liverpool
Brownlow Hill, Liverpool, L69 3GH, United Kingdom
s.fichera@liverpool.ac.uk

[3]University of Exeter
Stocker Rd, Exeter EX4 4PY, United Kingdom
a.vizzaccaro@exeter.ac.uk

[4]Airbus Operations Ltd, Bristol, BS34 7QQ, UK

Keywords: aeroelasticity, structural dynamics, hybrid testing

Abstract: Aeronautical structures, due to uncertainties and nonlinearities, require extensive experimental testing for both design and certification, especially concerning their aeroelastic behaviour. Such experimental procedures are conducted through both wind tunnel tests and flying prototypes. The latter introduces risks to personnel, entails higher costs, and provides considerably less control over external factors. At the same time, wind tunnel tests offer safety, affordability, repeatability, and control over external variables. However, due to the limitations of the wind tunnel test section, only scaled models or limited portions of the whole structure can be tested, resulting in a lack of interaction with surrounding aero-structural systems. Hybrid Testing (HT) is an advanced experimental technique in structural engineering that combines physical testing with numerical simulations to assess the behaviour of complex structures and systems under various loading conditions. In HT, the structure of interest is divided into physical and numerical substructures and then combined to form a hybrid structure reproducing the behavior of the original system. In the existing literature, HT has been primarily applied to academic simplified aeroelastic systems. This work aims to evaluate the feasibility of HT for aeroelastic industrial applications, considering a more realistic model. To this end, an aeroelastic straight untapered half-wing is examined. In this work, both virtual and physical substructures are simulated. A transfer system ensures force and displacement compatibility between the numerical and physical substructures through a control system employing sensors and actuators at the interface. Time delay and bandwidth limitations associated with the transfer system are modelled and investigated.

1 INTRODUCTION

Experimental testing of engineering structures has always been, and will continue to remain an integral part of the product development cycle, from the design stages through to commercialisation of the end product. Whilst in many cases it will not be possible to completely substitute

experimentation without compromising safety and accuracy, there continues to be an unrelenting search for methods to reduce the extent of required experimentation and thereby reduce timescales and costs, in a safe and sustainable way. Real-time Hybrid testing (HT) is a technique that has attracted significant attention in the past few decades. Originally developed within the field of earthquake engineering, the approach has begun to find application within other engineering disciplines including within Aerospace Engineering. With this innovative approach, it is sought to couple experimental testing of a portion of the overall system, with a numerical model of the remainder of the system functioning in real-time, such that the net behaviour of the hybrid system replicates the behaviour of the complete physical system with good accuracy. A key advantage of the approach is the ability to test the physical sub-system at full scale, allowing more accurate representations of scale-dependent phenomena such as nonlinear behaviours of various types.

Since the origin of the technique, there have been significant contributions to the literature on HT addressing various aspects of the approach. Blakeborough et al. [1] present a brief overview of HT, and proceed to describe the main features of the method. A detailed account of HT is provided by Wagg et al. [2], where over eighty related references are provided, and the background of HT, comparisons with other well-known approaches such as Hardware-in-the-loop, some of the key practical considerations of the approach such as stability and robustness, and techniques for alleviating well-known issues with the method such as Delay Compensation are presented. Among the implementations of HT within aircraft-related aeroelastic systems is the work by Fagley et al. [3], investigating the aeroelastic behaviour of a cyber-physical flexible wing model, their setup allowed running the system at a larger number of parameter combinations than would have been possible in a purely experimental setup. Waghela et al. [4], compare the performance of PID control and H infinity control in the cyber-physical transfer system in their setup. Su and Song [5] implement HT on a cyber-physical aeroelastic system based on a typical section 2-D aerofoil; results are generated in simulation only. Ruffini et al. [6], implement HT on a cyber-physical system consisting of a (physical) flexible strut-braced wing and a (numerically modelled) vibration absorber, to investigate aeroelastic response under gust excitation. Taking inspiration from the testing of aircraft wings, Vizzaccaro et al. [7] develop an iterative HT approach based on harmonic excitation for systems operating at steady-state, and demonstrate the method via application to a cantilever beam system that represents an aircraft wing; the controller is designed within the Fourier domain rather than in real-time.

The present research is motivated by the strong potential of the HT approach to be adopted and developed within aircraft-related aeroelastic environments, which would pave the way for HT to ultimately be embraced by industry. The feasibility of employing HT within industrial aeroelastic applications will be assessed, by simulating the application of the method in an aeroelastic cantilever wing. Section 2 presents the mathematical formulation of HT, which is followed by a description of and results pertaining to the test case in Section 3. A summary of the main findings thus far is presented in the final Conclusions, in Section 4.

2 METHODOLOGY

In this section, the methodology proposed in this work is presented. Figure 1 shows a structured flowchart detailing the methodology of a hybrid testing approach for both virtual and physical structures. The process begins with extracting matrices from a NASTRAN model using DMAP, labelled "Nastran matrices" in the flowchart, and proceeds to the next step labelled "Divide bulk and interface dofs". This suggests an initial data structuring phase involving the partitioning of elements for physical parts and the numerical model. In the 'Static condensation' phase,

reduced-order modelling using ”Craig–Bampton” on the numerical model is carried out. In this work, proportional control is used to ensure that the displacements on the virtual and physical interfaces are equal. Proportional control introduces a force proportional to the error, which is the difference between the displacement of the virtual interface and the physical interface. To implement this, nodes located at the interfaces between the physical and numerical models are defined and connected using a rigid spring element (a spring with high stiffness values). This setup is illustrated in the figure as 'Connect virtual and physical structure with rigid element'. Hybrid testing is then performed on these assembled models and the details are explained in the following. It should be noted that, in this section, the methodology is demonstrated for a dynamical system, but it can also be extended to a dynamic aeroelastic system.

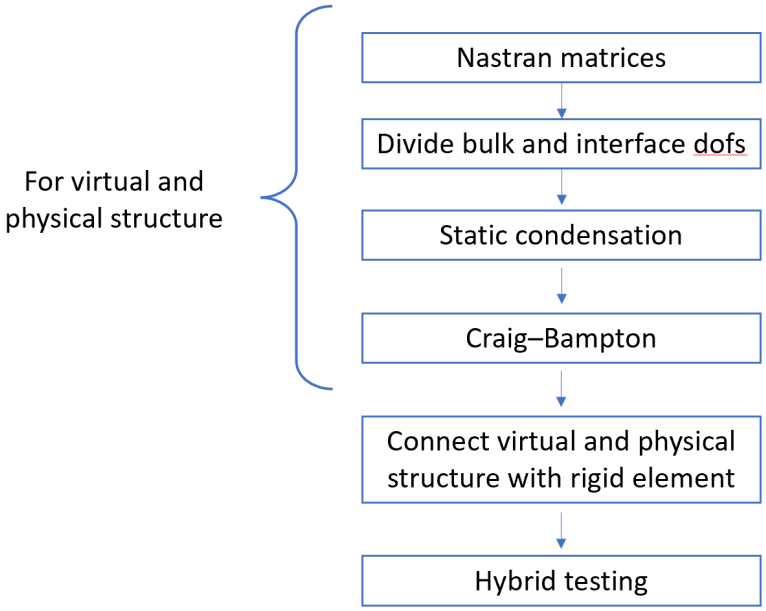

Figure 1: *Proposed Methodology*

The dynamic equation of motion for the complete structure can be expressed as a system of linear time-invariant ordinary differential equations (ODEs):

$$\mathbf{M}\ddot{\mathbf{x}} + \mathbf{C}\dot{\mathbf{x}} + \mathbf{K}\mathbf{x} = \mathbf{f}^e \tag{1}$$

where $\mathbf{M} \in \mathbb{R}^{n\times n}$, $\mathbf{C} \in \mathbb{R}^{n\times n}$, and $\mathbf{K} \in \mathbb{R}^{n\times n}$ represent the mass, damping, and stiffness matrices of the structure, respectively. $\mathbf{x} \in \mathbb{R}^{n\times 1}$ is the response vector, $\mathbf{f}^e \in \mathbb{R}^{n\times 1}$ is a generic external forcing vector and n denotes the number of degrees of freedom. In this paper, where the method presented here is applied to an aeroelastic system modelled using strip theory, the aerodynamic terms are initially included as part of $\mathbf{f}^e$, and thereafter moved to the left hand side of the equation where they appear as aerodynamic damping and aerodynamic stiffness related terms, which are then incorporated into the overall damping and stiffness matrices $\mathbf{C}$ and $\mathbf{K}$ respectively.

The original structure, modelled as Eq. (1), is divided into a physical model (denoted by subscript P) and a virtual model (denoted by subscript V). The physical and virtual models each include two sets of degrees of freedom. The first set refers to those nodes in the bulk of the substructure (indicated by subscript b) and those located at the interface (indicated by subscript i). Obviously, the degrees of freedom at the interface are identical and represent one set of

nodes in the original models before being divided into two models, i.e., physical and virtual. The equilibrium equations for the physical substructure may be written as

$$\begin{bmatrix}\mathbf{M}_{Pbb} & \mathbf{M}_{Pbi}\\ \mathbf{M}_{Pib} & \mathbf{M}_{Pii}\end{bmatrix}\begin{Bmatrix}\ddot{\mathbf{x}}_{Pb}\\ \ddot{\mathbf{x}}_{Pi}\end{Bmatrix}+\begin{bmatrix}\mathbf{C}_{Pbb} & \mathbf{C}_{Pbi}\\ \mathbf{C}_{Pib} & \mathbf{C}_{Pii}\end{bmatrix}\begin{Bmatrix}\dot{\mathbf{x}}_{Pb}\\ \dot{\mathbf{x}}_{Pi}\end{Bmatrix}+\begin{bmatrix}\mathbf{K}_{Pbb} & \mathbf{K}_{Pbi}\\ \mathbf{K}_{Pib} & \mathbf{K}_{Pii}\end{bmatrix}\begin{Bmatrix}\mathbf{x}_{Pb}\\ \mathbf{x}_{Pi}\end{Bmatrix}=\begin{Bmatrix}\mathbf{f}^{e}_{Pb}\\ \mathbf{f}^{e}_{Pi}+\mathbf{f}^{i}_{Pi}\end{Bmatrix} \quad (2)$$

where $\mathbf{x}_{Pb}$ and $\mathbf{x}_{Pi}$ are the vectors of the physical bulk and interface degrees of freedom, respectively. The superscripts e and i denote the external and internal forces, respectively. Similarly for the virtual substructure:

$$\begin{bmatrix}\mathbf{M}_{Vii} & \mathbf{M}_{Vib}\\ \mathbf{M}_{Vbi} & \mathbf{M}_{Vbb}\end{bmatrix}\begin{Bmatrix}\ddot{\mathbf{x}}_{Vi}\\ \ddot{\mathbf{x}}_{Vb}\end{Bmatrix}+\begin{bmatrix}\mathbf{C}_{Vii} & \mathbf{C}_{Vib}\\ \mathbf{C}_{Vbi} & \mathbf{C}_{Vbb}\end{bmatrix}\begin{Bmatrix}\dot{\mathbf{x}}_{Vi}\\ \dot{\mathbf{x}}_{Vb}\end{Bmatrix}+\begin{bmatrix}\mathbf{K}_{Vii} & \mathbf{K}_{Vib}\\ \mathbf{K}_{Vbi} & \mathbf{K}_{Vbb}\end{bmatrix}\begin{Bmatrix}\mathbf{x}_{Vi}\\ \mathbf{x}_{Vb}\end{Bmatrix}=\begin{Bmatrix}\mathbf{f}^{e}_{Vi}+\mathbf{f}^{i}_{Vi}\\ \mathbf{f}^{e}_{Vb}\end{Bmatrix} \quad (3)$$

where $\mathbf{x}_{Vb}$ and $\mathbf{x}_{Vi}$ are the vectors of the virtual bulk and interface degrees of freedom, respectively.

One significant challenge in using industrial-scale models is their large dimensions and the impact of their computational time on live interactions between physical part and numerical models. It is crucial to consider reduced-order modeling to address this issue in hybrid testing. For this purpose, the Craig-Bampton transformation is applied to both sets of equations introduced in (2) and (3). The displacement transformation of the Craig-Bampton method [8] reduces the computational complexity of large finite element models by employing a combination of fixed-interface normal modes $\mathbf{\Phi}_b$ and interface constraint modes $\mathbf{\Psi}_{bi}$, and takes the form

$$\begin{Bmatrix}\boldsymbol{x}_b\\ \boldsymbol{x}_i\end{Bmatrix}=\begin{bmatrix}\mathbf{\Phi}_b & \mathbf{0}\\ \mathbf{\Psi}_{bi} & \mathbf{I}\end{bmatrix}\begin{Bmatrix}\boldsymbol{\xi}_b\\ \boldsymbol{x}_i\end{Bmatrix} \quad (4)$$

where $\boldsymbol{\xi}_b$ are the generalized coordinates. The Craig-Bampton transformation matrix is

$$\mathbf{T}^{cb}=\begin{bmatrix}\mathbf{\Phi}_b & \mathbf{0}\\ \mathbf{\Psi}_{bi} & \mathbf{I}\end{bmatrix} \quad (5)$$

It is important to note that only the degrees of freedom corresponding to the bulk parts of the model are used for reduced-order modelling. Using the Craig-Bampton transformation matrix, Equation (2) becomes:

$$\begin{bmatrix}\hat{\mathbf{M}}_{Pbb} & \hat{\mathbf{M}}_{Pbi}\\ \hat{\mathbf{M}}_{Pib} & \hat{\mathbf{M}}_{Pii}\end{bmatrix}\begin{Bmatrix}\ddot{\boldsymbol{\xi}}_{Pb}\\ \ddot{\mathbf{x}}_{Pi}\end{Bmatrix}+\begin{bmatrix}\hat{\mathbf{C}}_{Pbb} & \mathbf{0}\\ \mathbf{0} & \hat{\mathbf{C}}_{Pii}\end{bmatrix}\begin{Bmatrix}\dot{\boldsymbol{\xi}}_{Pb}\\ \dot{\mathbf{x}}_{Pi}\end{Bmatrix}+\begin{bmatrix}\hat{\mathbf{K}}_{Pbb} & \mathbf{0}\\ \mathbf{0} & \hat{\mathbf{K}}_{Pii}\end{bmatrix}\begin{Bmatrix}\boldsymbol{\xi}_{Pb}\\ \mathbf{x}_{Pi}\end{Bmatrix}=\begin{Bmatrix}\hat{\mathbf{f}}^{e}_{Pb}\\ \mathbf{f}^{e}_{Pi}+\mathbf{f}^{i}_{Pi}\end{Bmatrix} \quad (6)$$

where the transformation matrix $\mathbf{T}^{cb}_{P}$ was used and $\boldsymbol{\xi}_{Pb}$ are the modal coordinates of the bulk degrees of freedom. Following the same procedure, equation (3) becomes

$$\begin{bmatrix}\hat{\mathbf{M}}_{Vii} & \hat{\mathbf{M}}_{Vib}\\ \hat{\mathbf{M}}_{Vbi} & \hat{\mathbf{M}}_{Vbb}\end{bmatrix}\begin{Bmatrix}\ddot{\mathbf{x}}_{Vi}\\ \ddot{\boldsymbol{\xi}}_{Vb}\end{Bmatrix}+\begin{bmatrix}\hat{\mathbf{C}}_{Vii} & \mathbf{0}\\ \mathbf{0} & \hat{\mathbf{C}}_{Vbb}\end{bmatrix}\begin{Bmatrix}\dot{\mathbf{x}}_{Vi}\\ \dot{\boldsymbol{\xi}}_{Vb}\end{Bmatrix}+\begin{bmatrix}\hat{\mathbf{K}}_{Vii} & \mathbf{0}\\ \mathbf{0} & \hat{\mathbf{K}}_{Vbb}\end{bmatrix}\begin{Bmatrix}\mathbf{x}_{Vi}\\ \boldsymbol{\xi}_{Vb}\end{Bmatrix}=\begin{Bmatrix}\mathbf{f}^{e}_{Vi}+\mathbf{f}^{i}_{Vi}\\ \hat{\mathbf{f}}^{e}_{Vb}\end{Bmatrix} \quad (7)$$

where the transformation matrix $\mathbf{T}^{cb}_{V}$ was used and $\boldsymbol{\xi}_{Vb}$ are the modal coordinates of the bulk degrees of freedom.

For the two systems to be connected, the internal interface forces have to be balanced

$$\mathbf{f}^{i}_{Vi}=-\mathbf{f}^{i}_{Pi}, \quad (8)$$

and the interface displacements have to be equal

$$\mathbf{x}_{Pi} = \mathbf{x}_{Vi}. \tag{9}$$

There are different strategies to impose these conditions but here we choose to simply regularise the problem and impose an a very stiff connection between the physical and virtual interface degrees of freedom, which leads to:

$$\mathbf{f}^i_{Vi} = -\mathbf{f}^i_{Pi} = \mathbf{K}_{\text{rigid}}(\mathbf{x}_{Pi} - \mathbf{x}_{Vi}) \tag{10}$$

where $\mathbf{K}_{\text{rigid}}$ is an identity matrix with the value of stiffness defined to ensure $\mathbf{x}_{Pi}$ and $\mathbf{x}_{Vi}$ have nearly the same dynamics. In this way, the interface forces (and moments) are automatically balanced and the interface error on displacements (and rotations) becomes smaller as the connection stiffnesses increase. From a control point of view, this is equivalent to use a simple proportional controller with high control gain.

The combined hybrid system reads:

$$\begin{bmatrix} \hat{\mathbf{M}}_{Pbb} & \hat{\mathbf{M}}_{Pbi} & \mathbf{0} & \mathbf{0} \\ \hat{\mathbf{M}}_{Pib} & \hat{\mathbf{M}}_{Pii} & \mathbf{0} & \mathbf{0} \\ \mathbf{0} & \mathbf{0} & \hat{\mathbf{M}}_{Vii} & \hat{\mathbf{M}}_{Vib} \\ \mathbf{0} & \mathbf{0} & \hat{\mathbf{M}}_{Vbi} & \hat{\mathbf{M}}_{Vbb} \end{bmatrix} \begin{Bmatrix} \ddot{\boldsymbol{\xi}}_{Pb} \\ \ddot{\mathbf{x}}_{Pi} \\ \ddot{\mathbf{x}}_{Vi} \\ \ddot{\boldsymbol{\xi}}_{Vb} \end{Bmatrix} + \begin{bmatrix} \hat{\mathbf{C}}_{Pbb} & \mathbf{0} & \mathbf{0} & \mathbf{0} \\ \mathbf{0} & \hat{\mathbf{C}}_{Pii} & \mathbf{0} & \mathbf{0} \\ \mathbf{0} & \mathbf{0} & \hat{\mathbf{C}}_{Vii} & \mathbf{0} \\ \mathbf{0} & \mathbf{0} & \mathbf{0} & \hat{\mathbf{C}}_{Vbb} \end{bmatrix} \begin{Bmatrix} \dot{\boldsymbol{\xi}}_{Pb} \\ \dot{\mathbf{x}}_{Pi} \\ \dot{\mathbf{x}}_{Vi} \\ \dot{\boldsymbol{\xi}}_{Vb} \end{Bmatrix} + \\ + \begin{bmatrix} \hat{\mathbf{K}}_{Pbb} & \mathbf{0} & \mathbf{0} & \mathbf{0} \\ \mathbf{0} & \hat{\mathbf{K}}_{Pii} + \mathbf{K}_{\text{rigid}} & -\mathbf{K}_{\text{rigid}} & \mathbf{0} \\ \mathbf{0} & -\mathbf{K}_{\text{rigid}} & \hat{\mathbf{K}}_{Vii} + \mathbf{K}_{\text{rigid}} & \mathbf{0} \\ \mathbf{0} & \mathbf{0} & \mathbf{0} & \hat{\mathbf{K}}_{Vbb} \end{bmatrix} \begin{Bmatrix} \boldsymbol{\xi}_{Pb} \\ \mathbf{x}_{Pi} \\ \mathbf{x}_{Vi} \\ \boldsymbol{\xi}_{Vb} \end{Bmatrix} = \begin{Bmatrix} \hat{\mathbf{f}}^e_{Pb} \\ \mathbf{f}^e_{Pi} \\ \mathbf{f}^e_{Vi} \\ \hat{\mathbf{f}}^e_{Vb} \end{Bmatrix} \tag{11}$$

To define the control scheme that will realise Eq. (11), we now split the physical and virtual systems as

$$\begin{bmatrix} \hat{\mathbf{M}}_{Pbb} & \hat{\mathbf{M}}_{Pbi} \\ \hat{\mathbf{M}}_{Pib} & \hat{\mathbf{M}}_{Pii} \end{bmatrix} \begin{Bmatrix} \ddot{\boldsymbol{\xi}}_{Pb} \\ \ddot{\mathbf{x}}_{Pi} \end{Bmatrix} + \begin{bmatrix} \hat{\mathbf{C}}_{Pbb} & \mathbf{0} \\ \mathbf{0} & \hat{\mathbf{C}}_{Pii} \end{bmatrix} \begin{Bmatrix} \dot{\boldsymbol{\xi}}_{Pb} \\ \dot{\mathbf{x}}_{Pi} \end{Bmatrix} + \begin{bmatrix} \hat{\mathbf{K}}_{Pbb} & \mathbf{0} \\ \mathbf{0} & \hat{\mathbf{K}}_{Pii} \end{bmatrix} \begin{Bmatrix} \boldsymbol{\xi}_{Pb} \\ \mathbf{x}_{Pi} \end{Bmatrix} = \begin{Bmatrix} \hat{\mathbf{f}}^e_{Pb} \\ \hat{\mathbf{f}}^e_{Pi} \end{Bmatrix} - \begin{Bmatrix} \mathbf{0} \\ \mathbf{F}_{\text{act}} \end{Bmatrix} \tag{12}$$

and

$$\begin{bmatrix} \hat{\mathbf{M}}_{Vii} & \hat{\mathbf{M}}_{Vib} \\ \hat{\mathbf{M}}_{Vbi} & \hat{\mathbf{M}}_{Vbb} \end{bmatrix} \begin{Bmatrix} \ddot{\mathbf{x}}_{Vi} \\ \ddot{\boldsymbol{\xi}}_{Vb} \end{Bmatrix} + \begin{bmatrix} \hat{\mathbf{C}}_{Vii} & \mathbf{0} \\ \mathbf{0} & \hat{\mathbf{C}}_{Vbb} \end{bmatrix} \begin{Bmatrix} \dot{\mathbf{x}}_{Vi} \\ \dot{\boldsymbol{\xi}}_{Vb} \end{Bmatrix} + \begin{bmatrix} \hat{\mathbf{K}}_{Vii} & \mathbf{0} \\ \mathbf{0} & \hat{\mathbf{K}}_{Vbb} \end{bmatrix} \begin{Bmatrix} \mathbf{x}_{Vi} \\ \boldsymbol{\xi}_{Vb} \end{Bmatrix} = \begin{Bmatrix} \hat{\mathbf{f}}^e_{Vi} \\ \hat{\mathbf{f}}^e_{Vb} \end{Bmatrix} + \begin{Bmatrix} \mathbf{F}_{\text{act}} \\ \mathbf{0} \end{Bmatrix} \tag{13}$$

where the actuation force acting on the interface of the physical system is defined as the interface force:

$$\mathbf{F}_{\text{act}} = \mathbf{K}_{\text{rigid}}(\mathbf{x}_{Pi} - \mathbf{x}_{Vi}). \tag{14}$$

Figure 2 shows a control system that incorporates interactions between the physical system and the virtual system, defined using Simulink. Initially, a gust input is fed to both the physical and virtual models, which corresponds to the external force in Eq. (12) and Eq. (13). The solution of the physical model (which, in real scenarios, involves actual experiments on the physical structure) determines the displacements at the physical interface $\mathbf{x}_{Pi}$. Simultaneously, the solution of the numerical model results in displacements at the virtual interface nodes $\mathbf{x}_{Pi}$.

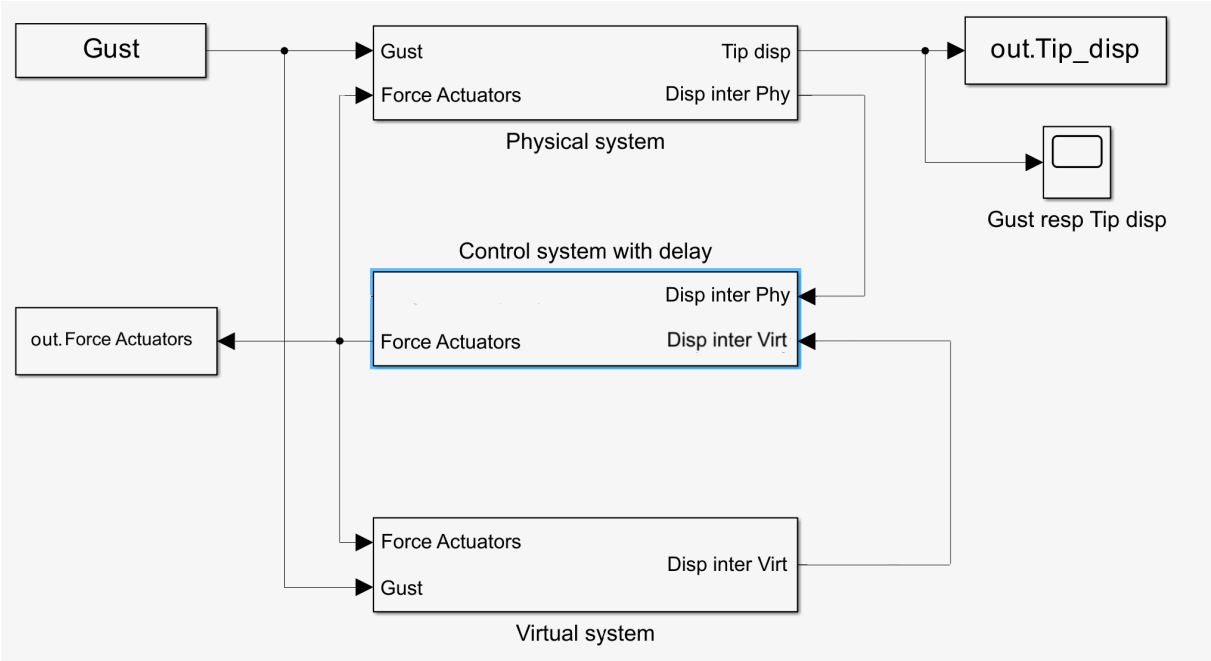

Figure 2: *Simulink model*

Both the physical and virtual nodes' displacements are fed into the control system to generate the actuation force $\mathbf{F}_{\text{act}}$, as defined in Equation 14. This actuation force is then inputted into the both substructures to minimize the discrepancy between the displacements at the virtual and physical interface nodes.

Delays associated with actuator forces and phase lag arising in measurements from sensors is an important practical consideration within HT, and is known to cause various undesirable dynamic phenomena including instability. Thus, accounting for these is a significant part of ensuring accuracy of the HT process. There are various combinations of delay and phase lag that may be modelled. In the present work, the focus has been placed on actuator delay. This control system includes a feedback mechanism with inherent delay applied to the actuator force signal, to mimic real life scenarios in which there will usually be a delay between when the required actuator forces are calculated and applied at the interface.In this work, the actuator delay has been modelled as a time delay by a certain amount of time τ (represented as $e^{-s\tau}$ in the Laplace domain).

3 TEST CASE

3.1 Hybrid testing for industrial applications – cantilever elastic wing

In this section, the approach introduced in Section 2 is applied to the aeroelastic equations of motion, presented as follows:

$$\mathbf{A}\ddot{\mathbf{x}} + (\rho V \mathbf{B} + \mathbf{D})\,\dot{\mathbf{x}} + \left(\rho V^2 \mathbf{C} + \mathbf{E}\right)\mathbf{x} = \mathbf{f} \tag{15}$$

In Eq. 15, $\mathbf{A}$, $\mathbf{D}$, and $\mathbf{E}$ represent the structural inertia, damping, and stiffness matrices, respectively, while $\mathbf{B}$ and $\mathbf{C}$ denote the aerodynamic damping and stiffness matrices. The vector $\mathbf{x}$ comprises physical coordinates, and the force vector $\mathbf{f}$ on the right-hand side can include contributions from trim, lift at zero incidence, the gravitational field, and gust effects on the

aerodynamic surfaces. In this case, the external force $\mathbf{f}$ is attributed to gusts, and the aerodynamic model uses strip theory, incorporating the lift coefficient curve with a slope of 2π.

The wing under investigation is a cantilevered, straight rectangular wing with a span of 0.6 metres and a chord of 0.2 metres. It consists of an aluminium spar with Young's modulus of 72 MPa and a density of 2700 kg/m^3. The spar features a cross-sectional design. Additionally, the wing includes seven 3D-printed airfoil sections, each weighing 0.01 kg. The design of the wing is similar to those previously studied by the authors [9–12]. The wing was modelled in Nastran using a stick model and concentrated masses representative of the Aerofoil sections. To simulate the actual behaviour of the wing, 1% proportional damping was incorporated. Figure 3 shows the elastic wing considered in this study. Table 1 summarises the main wing parameters. Following the methodology outlined in Section 2, the wing was divided into a physical model

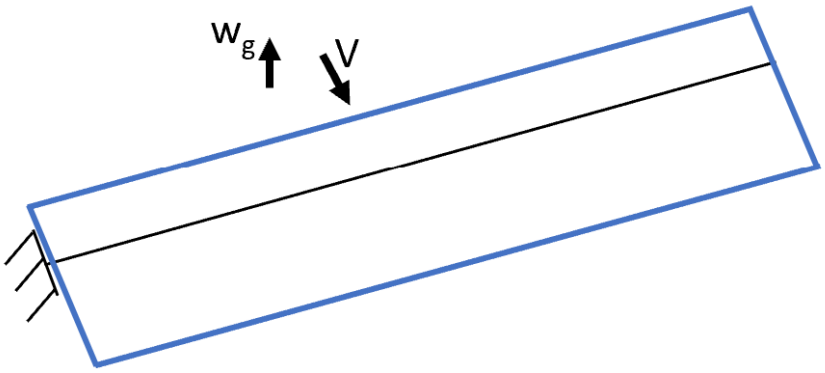

Figure 3: *Elastic wing considered for HT*

Span	0. 6 m
Chord	0.2 m
Airspeed	12 m/s
Structure	stick model
Aerodynamic model	strip theory

Table 1: Full wing parameters

and a virtual model. In the connection between the physical and the virtual system, a stiffness of 10^7 N/m was introduced at the displacement degrees of freedom and 10^7 Nm/rad was introduced at the rotational degrees of freedom. The virtual model comprises the first 0.5 m of the wing span, while the physical model represents the last 0.1 m. Figure 4 shows the wind divided into a virtual and a physical structure.

To ensure the hybrid testing procedure was implemented correctly, an eigenvalue analysis was performed on both the full system (using the Nastran sol103 analysis) and the hybrid testing system. Table 2 shows a comparison between the wing structural frequencies calculated by Nastran and those obtained by considering the two substructures connected with a rigid spring. The increased curvature of the wing mode shapes at higher frequencies results in greater discrepancies between the natural frequencies of the original model and the model with rigid spring elements.

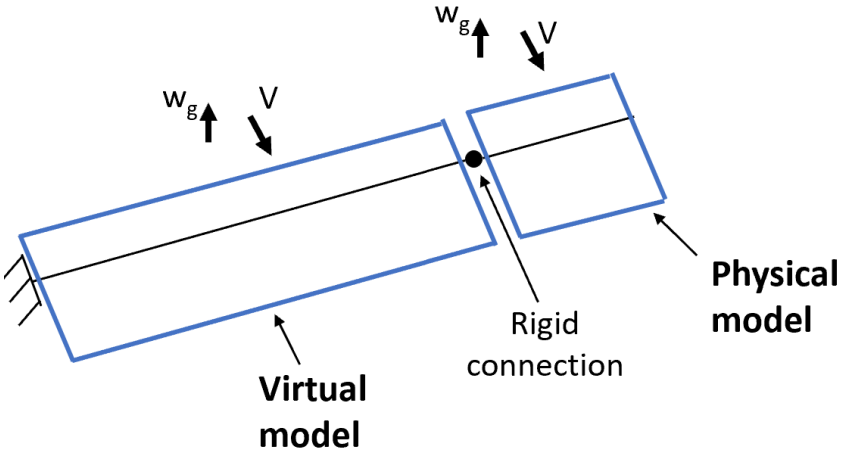

Figure 4: *Elastic wing considered for HT*

Nastran [Hz]	Substructuring [Hz]	Error
0.49	0.49	0%
1.26	1.26	0%
3.00	2.99	0.3%
7.65	7.66	0.1%
8.12	8.15	0.04%
20.79	22.42	7.8%

Table 2: Comparison full wing structural frequencies

3.2 Aeroelastic gust response

In this section, the wing tip displacement response of the wing at sea level, subjected to an airspeed of 12 m/s and a vertical gust, is demonstrated. Figure 5 illustrates the comparison between the vertical displacement of the wing tip for the full wing (reference) and the HT system (Simulink) in response to a sinusoidal gust of 1 m/s at 0.5 Hz. It is evident that the results of the two models, assuming zero delay, correspond closely, demonstrating the applicability of the proposed HT.

3.3 Effect of actuator delay

The effects of delays in force and moment actuators are examined in this section. As shown in Figure 6, lower values of time delays in the vertical force actuator at the interface do not significantly impact the HT model results when compared to the original model results. However, the results deteriorate at higher values of time delays, highlighting the importance of these effects in HT. The delay in force also affects the moment actuator force, as seen on the right-hand side of Figure 6. The delay in the moment actuator is further illustrated in Figure 7. The results indicate that delays in the moment actuator create higher levels of errors compared to delays in the vertical force. Figure 8 demonstrates the effects of delays in both force and moment actuators simultaneously, and as expected, the effects in this case are more pronounced.

The trends observed in the above results demonstrate how profoundly the performance of the HT scheme can be affected by actuator delay; thus, it is vital that (a) appropriate actuators with minimal delays and other undesirable dynamics are chosen, (b) suitable delay compensation techniques are implemented within the interface control system to alleviate the effects of actuator delay.

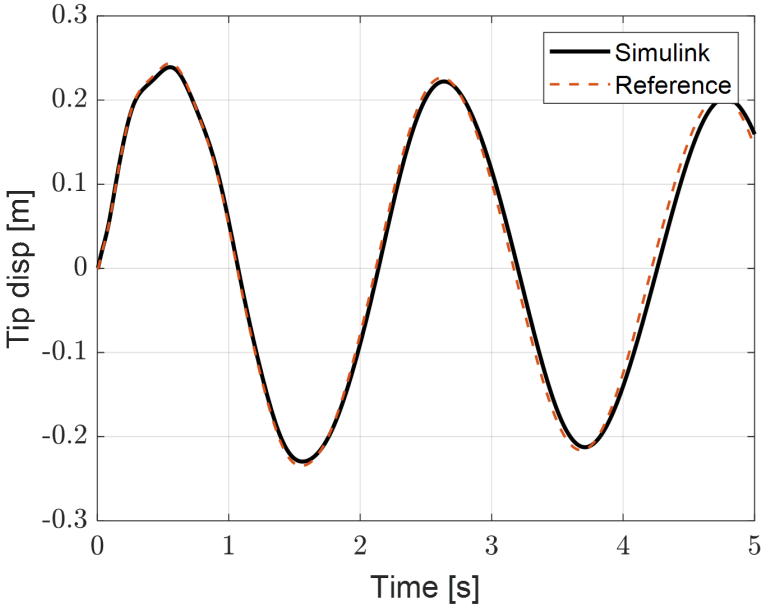

Figure 5: *Elastic wing gust response*

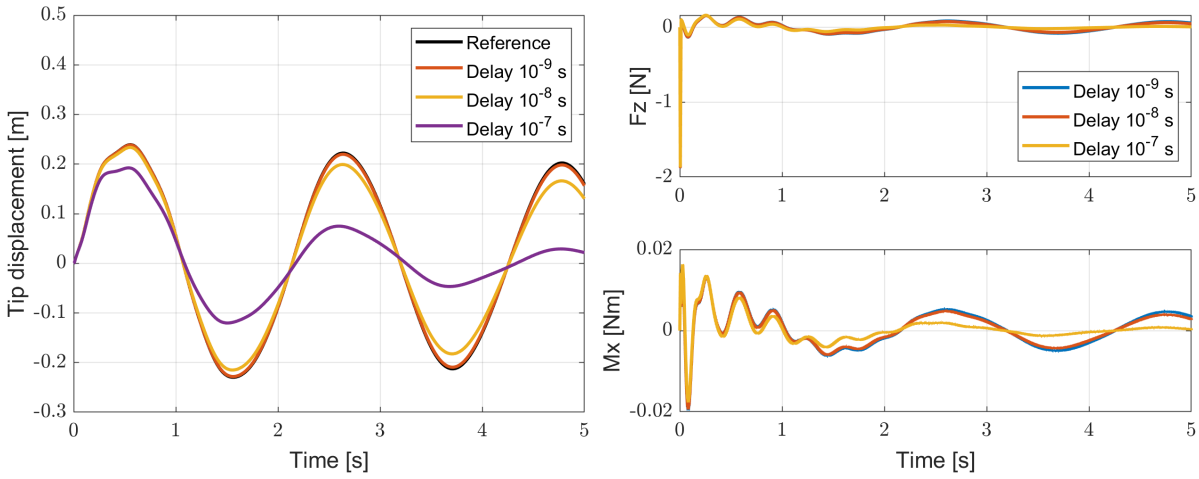

Wing gust response Actuators response

Figure 6: Gust response considering delay in the Fz actuator

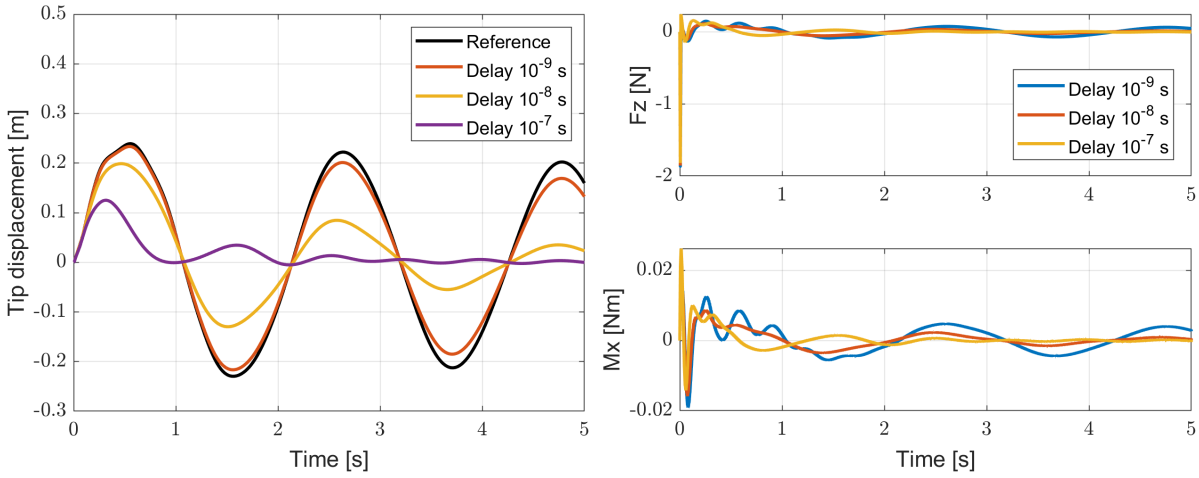

Wing gust response Actuators response

Figure 7: Gust response considering delay in the Mx actuator

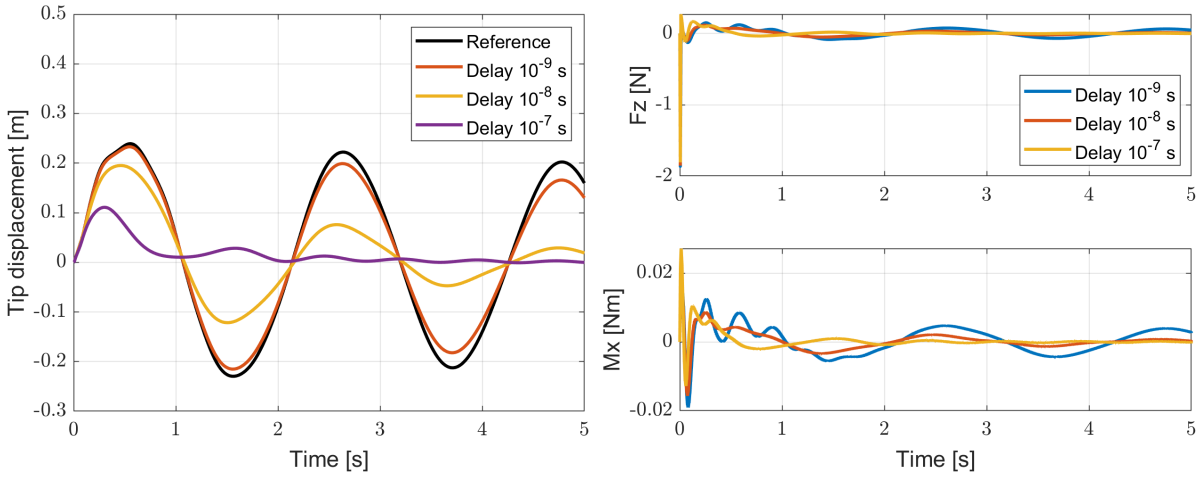

Wing gust response Actuators response

Figure 8: Gust response considering delay in the Fz and Mx actuators

4 CONCLUSION

This paper demonstrates the application of model reduction techniques in the hybrid testing (HT) of aeroelastic systems. HT has been widely used for systems with a small number of degrees of freedom. To the authors' knowledge, there has been no work on applying HT to more realistic test cases, which are necessary for the application of industrialised test cases. This paper presents preliminary results from efforts to address this gap. For model reduction of dynamical systems, the Craig-Bampton method was employed. Although the ultimate aim is to facilitate live interaction between the physical model and the numerical model, in this initial attempt, we used a realistic cantilever wing model divided into two sections. One part represents the numerical section, while the other mimics the physical structure. The connection between the two models is modelled using rigid spring elements that replicate the role of actuator forces, providing interaction forces between the numerical and physical components at the interface. It is assumed that sensors measuring the interface displacement feed into the control system, defining the actuator force. Results are demonstrated in an aeroelastic model of a cantilever wing and show excellent agreement between the original model results and HT results in the absence of any delay in actuator force. It highlights the significance of delays in actuation forces and how they can significantly deteriorate the effectiveness of HT results. Therefore, future work should focus on implementing delay compensation methods in actuation systems.

5 ACKNOWLEDGEMENT

The financial support provided by the EPSRC Impact Acceleration for Dr. Davide Balatti's secondment to Airbus is gratefully acknowledged.

6 REFERENCES

[1] Blakeborough, A., Williams, M., Darby, A., et al. (2001). The development of real-time substructure testing. *Philosophical Transactions of The Royal Society A: Mathematical, Physical and Engineering Sciences*, 359, 1869–1891. doi:10.1098/rsta.2001.0877.

[2] Wagg, D., Neild, S., and Gawthrop, P. (2008). *Real-Time Testing With Dynamic Substructuring*. Vienna: Springer Vienna. ISBN 978-3-211-09445-7, pp. 293–342. doi: 10.1007/978-3-211-09445-7_7.

[3] Fagley, C., Seidel, J., and McLaughlin, T. (2016). Cyber-physical flexible wing for aeroelastic investigations of stall and classical flutter. *Journal of Fluids and Structures*, 67, 34–47. ISSN 0889-9746. doi:10.1016/j.jfluidstructs.2016.07.021.

[4] Waghela, R., Bryant, M., and Wu, F. (2018). Control design in cyber-physical fluid-structure interaction experiments. *Journal of Fluids and Structures*, 82, 86–100. ISSN 0889-9746. doi:10.1016/j.jfluidstructs.2018.06.018.

[5] Su, W. and Song, W. (2019). A real-time hybrid aeroelastic simulation platform for flexible wings. *Aerospace Science and Technology*, 95, 105513. ISSN 1270-9638. doi:https://doi.org/10.1016/j.ast.2019.105513.

[6] Ruffini, V., Szczyglowski, C., Barton, D. A. W., et al. (2020). Real-time hybrid testing of strut-braced wing under aerodynamic loading using an electrodynamic actuator. *Experimental Techniques*, 44(6), 821–835. ISSN 0732-8818. doi:10.1007/s40799-020-00394-5.

[7] Vizzaccaro, A., Beregi, S., Barton, D., et al. Iterative method for real time hybrid testing: application to a cantilever beam with two controlled degrees of freedom.

[8] Craig Jr, R. R. and Kurdila, A. J. (2006). *Fundamentals of structural dynamics*. John Wiley & Sons.

[9] Balatti, D., Khodaparast, H. H., Friswell, M. I., et al. (2022). Aeroelastic model validation through wind tunnel testing of a wing with hinged wingtip. In *International Forum on Aeroelasticity and Structural Dynamics, Madrid, Spain*.

[10] Balatti, D., Ellis, J. D., Jiffri, S., et al. (2023). Active hinged wingtip for gust load alleviation and manoeuvres. In *AIAA SCITECH 2023 Forum*. p. 2567.

[11] Balatti, D., Khodaparast, H. H., Friswell, M. I., et al. (2023). Experimental and numerical investigation of an aircraft wing with hinged wingtip for gust load alleviation. *Journal of Fluids and Structures*, 119, 103892.

[12] Ellis, J. D., Balatti, D., Haddad Khodaparast, H., et al. (2023). Multiple-input, multiple-output linear and nonlinear active control of a flexible wing. In *AIAA SCITECH 2023 Forum*. p. 0375.

COPYRIGHT STATEMENT